INVERSE DESIGN OF DIELECTRIC MATERIALS BY TOPOLOGY OPTIMIZATION

AUTHOR(S):

Otomori, Masaki

Progress In Electromagnetics Research, Vol. 127, 93–120, 2012

INVERSE DESIGN OF DIELECTRIC MATERIALS BY TOPOLOGY OPTIMIZATION

M. Otomori[1,*], J. Andkjær[2], O. Sigmund[2], K. Izui[1], and S. Nishiwaki[1]

[1]Kyoto University, Yoshida Honmachi, Sakyo-ku, Kyoto 606-8501, Japan

[2]Technical University of Denmark, Nils Koppels Alle, Building 404, 2800 Kgs. Lyngby, Denmark

Abstract—The capabilities and operation of electromagnetic devices can be dramatically enhanced if artificial materials that provide certain prescribed properties can be designed and fabricated. This paper presents a systematic methodology for the design of dielectric materials with prescribed electric permittivity. A gradient-based topology optimization method is used to find the distribution of dielectric material for the unit cell of a periodic microstructure composed of one or two dielectric materials. The optimization problem is formulated as a problem to minimize the square of the difference between the effective permittivity and a prescribed value. The optimization algorithm uses the adjoint variable method (AVM) for the sensitivity analysis and the finite element method (FEM) for solving the equilibrium and adjoint equations, respectively. A Heaviside projection filter is used to obtain clear optimized configurations. Several design problems show that clear optimized unit cell configurations that provide the prescribed electric permittivity can be obtained for all the presented cases. These include the design of isotropic material, anisotropic material, anisotropic material with a non-zero off-diagonal terms, and anisotropic material with loss. The results show that the optimized values are in agreement with theoretical bounds, confirming that our method yields appropriate and useful solutions.

Received 5 February 2012, Accepted 23 March 2012, Scheduled 10 April 2012
* Corresponding author: Masaki Otomori (otomori.masaki.58r@st.kyoto-u.ac.jp).

1. INTRODUCTION

Artificial dielectric materials that are engineered to have an extreme dielectric constant are of great interest for improving electromagnetic devices such as electrostatic actuators, waveguides, antennas, etc. This paper presents a systematic design methodology for the microstructure design of composites made from two dielectric materials with different dielectric constants, or a single dielectric material and air. We use topology optimization to find the shape and distribution of dielectric elements that exhibits a prescribed desirable dielectric constant.

Topology optimization is the most flexible type of structural optimization because it allows topological changes as well as shape changes during the optimization process [1]. Topology optimization methods have been applied to a variety of problems such as electromagnetic problems (e.g., [2–5]), fluid dynamics problem (e.g., [6]), phononics [7] and others. Topology optimization has also been successfully applied to various microstructure design problems aiming to develop materials that have extreme properties such as a negative thermal expansion coefficient [8], a negative Poisson's ratio [9], and materials with a prescribed value of a constitutive tensor such as Young's modulus [10], magnetic permeability [11], a dielectric constant [12], and so on. These problems are called inverse homogenization problems [10].

There are various methods for obtaining an effective permittivity value for dielectric composites. Analytic methods such as the Clausius-Mossotti, Maxwell-Garnett, and Bruggeman formulas, which are also called mixing formulas, compute the effective permittivity of composites based on the volume of the inclusions [13], however the accuracy is valid only for certain inclusion shapes such as spheres, cylinders, and ellipsoids. A homogenization method such as a method based on asymptotic expansion [14, 15], and also an energy-based method [16], can be used when dealing with more complicated shapes where the effective properties are obtained based on the results of finite element analysis. In this study, an energy-based method is used to obtain the effective permittivity of the dielectric materials.

There is considerable literature on the investigation of the theoretical bounds for the effective properties of composites (e.g., [17]). The primal bounds for two-phase dielectric materials are given by arithmetic and harmonic means of each dielectric constant. Tighter bounds can be obtained based on certain available information about the composites, such as their volume fractions and/or isotropy. In this paper, we deal with two-dimensional design problems. To evaluate the permittivity values obtained in optimization, we derive the theoretical

bounds of the two-dimensional anisotropic effective property in the principal direction when that of the other principal direction is set to a prescribed value. Permittivity values obtained in optimizations are compared with these derived theoretical bounds.

In a previous study on the microstructure design of dielectric materials [12], a genetic algorithm (GA) was used in the optimization method. However, meta-heuristic approaches such as GAs, Particle Swarm Optimization (PSO), and Simulated Annealing (SA) are generally not suitable for topology optimization since the number of design variables is usually so large that the optimization becomes too computationally costly [18]. Hence in [12] design resolution was limited to extremely coarse discretizations. In this work, a gradient-based topology optimization method is used to find the distribution of dielectric material for the unit cell of a periodic microstructure, where densities are updated based on the sensitivities. The computation of sensitivities is significantly streamlined by using the adjoint variable method (AVM). In this way, we are able to solve problems with very fine discretizations and hence obtain accurate results and detailed boundary descriptions. The objective of the optimization is to design dielectric materials that exhibit a prescribed effective permittivity. Therefore, the optimization problem is formulated as a problem to minimize the square of the difference between the effective permittivity and a prescribed value. The optimization algorithm uses the finite element method (FEM) for solving the equilibrium and adjoint equations, respectively. A Heaviside projection filter [20] is used to obtain clear optimized configurations. We study several design problems including the design of an isotropic material, an anisotropic material, an anisotropic material with non-zero off-diagonal terms, and an anisotropic material with loss.

The rest of this paper is as follows. Section 2 describes the formulation of the homogenization method for obtaining the effective permittivity, and the optimization problem for the design of dielectric metamaterials. Section 3 discusses the theoretical bounds of the effective properties for two-phase composites. Section 4 describes the numerical implementation based on the formulation of the optimization problem, which uses the FEM and AVM to compute the sensitivity. Finally, several numerical examples are provided to confirm the validity and utility of the presented method.

2. FORMULATION

2.1. Effective Permittivity

In this study, the electrostatic effective permittivity is obtained on the basis of the energy-based approach that employ conductivity average theorems [16] (see also [10]), where the effective permittivities are expressed in terms of mutual energies as follows. This method assume that the mutual energies accumulated in the original unit cell and in the homogenized cell are equivalent. The mutual energy accumulated in the original unit cell is given as

$$Q_{ij} = \frac{1}{2}\int_{\Omega} \epsilon_r \nabla\bar{\phi}_i \cdot \nabla\phi_j d\Omega, \tag{1}$$

where ϵ_r represents the element of electric permittivity tensor and ϕ_i and ϕ_j are the electric potentials obtained when an electric voltage is applied in the x_i and x_j directions, respectively (Figure 1), where ij=11, 12, 21, 22, and $\bar{\phi}_i$ denotes the conjugate complex number of ϕ_i. On the other hand, the mutual energy accumulated in the homogenized cell is given as

$$Q_{ij}^H = \frac{1}{2}\epsilon_{\text{eff},\,ij} V_i^0 V_j^0 V, \tag{2}$$

where V is the volume and V_i^0 is the applied voltage defined in a boundary condition that produce homogeneous fields. By assuming $Q_{ij} = Q_{ij}^H$, the elements of the effective permittivity tensor, $\epsilon_{\text{eff},\,ij}$ in Eq. (2), are determined as follows.

$$\epsilon_{\text{eff}} = \begin{bmatrix} \epsilon_{\text{eff},\,11} & \epsilon_{\text{eff},\,12} \\ \epsilon_{\text{eff},\,21} & \epsilon_{\text{eff},\,22} \end{bmatrix}, \tag{3}$$

where

$$\epsilon_{\text{eff},\,11} = \frac{1}{{V_1^0}^2 V}\int_{\Omega} \epsilon_r(\mathbf{x})\nabla\bar{\phi}_1(\mathbf{x}) \cdot \nabla\phi_1(\mathbf{x})\, d\Omega \tag{4}$$

$$\epsilon_{\text{eff},\,22} = \frac{1}{{V_2^0}^2 V}\int_{\Omega} \epsilon_r(\mathbf{x})\nabla\bar{\phi}_2(\mathbf{x}) \cdot \nabla\phi_2(\mathbf{x})\, d\Omega \tag{5}$$

$$\epsilon_{\text{eff},\,12} = \frac{1}{V_1^0 V_2^0 V}\int_{\Omega} \epsilon_r(\mathbf{x})\nabla\bar{\phi}_2(\mathbf{x}) \cdot \nabla\phi_1(\mathbf{x})\, d\Omega \tag{6}$$

$$\epsilon_{\text{eff},\,21} = \frac{1}{V_1^0 V_2^0 V}\int_{\Omega} \epsilon_r(\mathbf{x})\nabla\bar{\phi}_1(\mathbf{x}) \cdot \nabla\phi_2(\mathbf{x})\, d\Omega, \tag{7}$$

The electric potential ϕ_i are obtained by solving the following governing equation using the FEM.

$$\nabla \cdot [\epsilon_r(\mathbf{x})\nabla\phi_i(\mathbf{x})] = 0, \tag{8}$$

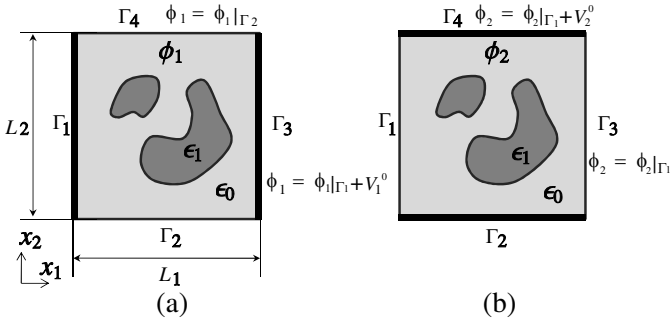

Figure 1. Analysis model and boundary conditions for the case of an electric voltage applied in (a) the horizontal direction, and (b) the vertical direction.

The left and right boundaries, and the upper and lower boundaries are, respectively, set to a periodic boundary condition as follows, in the case when an electric voltage is applied in the horizontal direction (Figure 1(a)).

$$\phi_1(x_1, x_2) = \phi_1(x_1 - L_1, x_2) + V_1^0 \quad \text{on } \Gamma_3 \tag{9}$$

$$\phi_1(x_1, x_2) = \phi_1(x_1, x_2 - L_2) \quad \text{on } \Gamma_4, \tag{10}$$

where V_1^0 is an applied voltage in the horizontal direction and, L_1 and L_2 are the unit cell lengths in the x_1 and x_2 directions, respectively.

The left and right boundaries, and the upper and lower boundaries are, respectively, set to a periodic boundary condition as follows, in the case when an electric voltage is applied in the vertical direction (Figure 1(b)).

$$\phi_2(x_1, x_2) = \phi_2(x_1 - L_1, x_2) \quad \text{on } \Gamma_3 \tag{11}$$

$$\phi_2(x_1, x_2) = \phi_2(x_1, x_2 - L_2) + V_2^0 \quad \text{on } \Gamma_4, \tag{12}$$

where V_2^0 is an applied voltage in the vertical direction. The effective permittivities are obtained by substituting obtained electric potentials into Eqs. (4)–(7).

2.2. Design Variables

In this work, the distribution of dielectric material inside the fixed design domain is expressed using relative element densities $\tilde{\rho}_e \in [0, 1]$. That is, the relative electric permittivity ϵ_r inside the fixed design domain is defined using $\tilde{\rho}_e$ following the concept of the SIMP method.

$$\epsilon_r = (\epsilon_1 - \epsilon_0)\, \tilde{\rho}_e^p + \epsilon_0, \tag{13}$$

where ϵ_1 is the relative permittivity of the dielectric material, ϵ_0 is the relative permittivity of the background material, and p is a penalization parameter. For problems that have an active volume constraint, a large value of $p > 1$ penalizes intermediate element densities, since the volume is proportional to $\tilde{\rho}_e$ but the permittivity values fall below the line of proportionality. The parameter $p \geq 3$ is typically used in structural optimization problems, since the bulk modulus and shear modulus of interpolated stiffness tensor are required to satisfy the Hashin-Shtrikman bounds, which isotropic materials should satisfy [19]. Here, we use $p = 3$ in the following numerical examples. It is because the profile of interpolated permittivity by $p = 3$ respect to the element density is similar to, even though it is not the same as, that of the Hashin-Strikman bounds when the loss of dielectric materials is small.

To ensure that the optimal design is independent of the mesh, and to obtain a clear optimal configuration, the Heaviside projection filter is used in this work [20]. Using this filter, the relative element densities $\tilde{\rho}_e$ can be computed as shown in the following procedures. First, intermediate variables μ_e are computed using design variables ρ_e that are typically located in nodes or the center of the finite elements, as follows.

$$\mu_e = \sum_{j \in N^e} \rho_e w / \sum_{j \in N^e} w, \tag{14}$$

where N^e is the neighborhood of elements specified by a circle with the given filter radius, and w is a weighting function that imposes higher weights for closer design variables. The relative element densities are then obtained using the Heaviside function as follows.

$$\tilde{\rho}_e = H_s(\mu_e) = 1 - e^{-\beta \mu_e} + \mu_e e^{-\beta}, \tag{15}$$

where β is a parameter that adjusts the curvature of the Heaviside function. To ensure stable convergence of the optimization, the magnitude of parameter β is gradually increased from 1 to sufficiently large value (e.g., 500) during the optimization procedure. Published references provide more details concerning the use of density filters [20, 21].

2.3. Optimization Problem

Here, we discuss the formulation of the optimization problem that will be applied to the dielectric material design problems. The purpose of the optimization is to obtain layouts of dielectric material that achieve the desired dielectric permittivity. Thus, the objective of the optimization problem can be formulated as to minimize the square of

the difference between the target permittivity and obtained effective permittivity. The optimization problem is described as follows.

$$\inf_{\rho_e} \qquad F(\rho_e) = \log \sum_{ij} \left| \epsilon^*_{\text{eff, ij}} / \epsilon^*_{\text{tar, ij}} - 1 \right|^2 \tag{16}$$

$$\text{subject to} \quad G = \frac{1}{V_D} \int_D \tilde{\rho}_e d\Omega - V_{\max} \leq 0 \tag{17}$$

$$\text{Poisson equation: Eq. (8)} \tag{18}$$

$$\text{Boundary conditions: Eqs.(9)–(12)} \tag{19}$$

where ϵ_{eff} and ϵ_{tar} respectively represent the effective permittivity and the target permittivity. The * denotes the use of either $'$ or $''$ that apply to the real or imaginary part of the effective permittivity, respectively. The subscript $ij = 11, 12, 21, 22$ denotes the elements of the dielectric tensor. V_D is the volume of the fixed design domain and $V_{\max}$ is the upper limit of volume fraction. Note that the logarithm of the sum of the differences is used as an objective functional to obtain better numerical scaling. When the differences become smaller during optimization, the magnitude of the sensitivities also diminish, which slows convergence.

2.4. Sensitivity Analysis

The sensitivities of the objective functional for the gradient-based topology optimization are obtained using the adjoint variable method (AVM). The governing equation is discretized and solved using the FEM. The discretized governing equation can be described as follows.

$$\mathbf{S}\phi_i = \mathbf{f}, \tag{20}$$

where $\mathbf{S}$ is the stiffness matrix and $\mathbf{f}$ is the load vector. The sensitivity of the objective functional F is then given as

$$\frac{dF}{d\rho} = \frac{\partial F}{\partial \rho} + 2Re\left(\lambda^T \left(\frac{\partial \mathbf{S}}{\partial \rho}\phi_i - \frac{\partial \mathbf{f}}{\partial \rho}\right)\right), \tag{21}$$

where λ is an adjoint variable. The adjoint variable λ is obtained by solving following adjoint problem.

$$\mathbf{S}^T\lambda = -\frac{\partial F}{\partial \phi_i}. \tag{22}$$

With A as the integrand of the objective functional, the derivative of the objective functional with respect to the state variable $\frac{\partial F}{\partial \phi_i}$ can be computed directly as follows.

$$\frac{\partial F}{\partial \phi_i} = \frac{1}{V^2} \int_D \left(\frac{\partial A}{\partial \phi_i} + \frac{\partial A}{\partial \nabla \phi_i} \cdot \nabla\right) dD, \tag{23}$$

where,

$$\frac{\partial A}{\partial \phi_i} = 0 \tag{24}$$

$$\frac{\partial A}{\partial \nabla \phi_i} = \epsilon_r \nabla \bar{\phi}_i. \tag{25}$$

In Eq. (21), $\frac{\partial \mathbf{f}}{\partial \rho} = 0$ since the applied voltage is independent with respect to the design variables. Computation of the derivative using Eq. (21) can be simplified by following Olesen's implementation technique [22].

3. THEORETICAL BOUNDS

In this section, the theoretical bounds of the effective permittivity for two-phase dielectric composites are discussed.

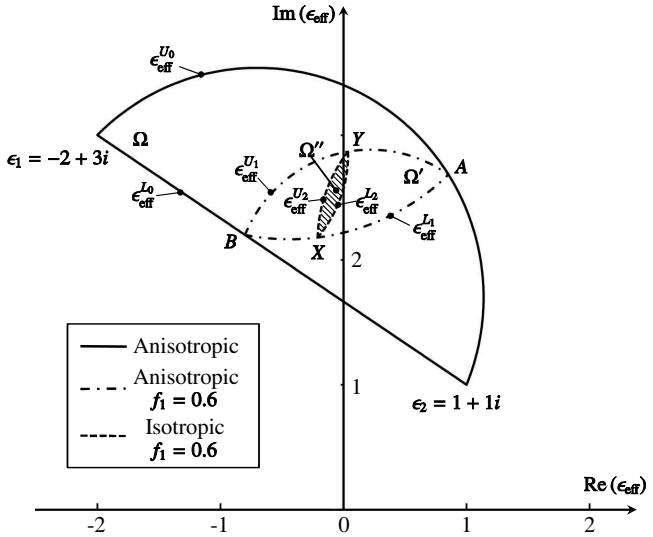

Figure 2. Bounds of effective permittivity for two constituent materials with properties $\epsilon_1 = -2 + 3i$ and $\epsilon_2 = 1 + 1i$. In the absence of specific information concerning the dielectric materials, the effective permittivity is confined to the region Ω. If the volume fraction of phase 1 is $f_1 = 0.6$, the effective permittivity is confined to the region Ω'. Furthermore, if the composite is a two-dimensional isotropic material, the effective permittivity is confined to the region Ω''.

3.1. Review of Theoretical Bounds of Effective Permittivity for Two-phase Composite Material

3.1.1. Bounds of Complex Value Effective Permittivity

Let ϵ_{eff} be the effective permittivity of a two-phase composite with complex dielectric constants ϵ_1 and ϵ_2. The analytical bounds of ϵ_{eff} can be illustrated as shown in Figure 2. Here, as an example, the dielectric constants for phases 1 and 2 are set to $\epsilon_1 = -2 + 3i$ and $\epsilon_2 = 1 + 1i$, respectively, and the volume fraction for phase 1 is set to 0.6 for bounds $\Omega^{'}$, $\Omega^{''}$, (the same example as Chap. 27 in [17]). These bounds are obtained as follows. We note that for composites made from a single dielectric material and air, the bounds are obtained by setting $\epsilon_2 = 1$.

In the absence of specific information concerning the topological distribution of the constituent, the corresponding bounds are the Wiener harmonic and arithmetic mean bounds expressed by following equations.

$$\epsilon_{\text{eff}}^{U_0}(v) = \left(\frac{v}{\epsilon_1} + \frac{1-v}{\epsilon_2}\right)^{-1} \tag{26}$$

$$\epsilon_{\text{eff}}^{L_0}(w) = w\epsilon_1 + (1-w)\epsilon_2, \tag{27}$$

as parameters v and w are varied from 0 to 1.

The boundary $\epsilon_{\text{eff}}^{U_0}(v)$ represents the composite as a laminate material oriented so that the applied field V^0 is parallel to the direction of lamination (see Figure 3(a)). On the other hand, boundary $\epsilon_{\text{eff}}^{L_0}(w)$ represents the composite as a laminate material oriented so that the applied field V^0 is orthogonal to the direction of lamination (see Figure 3(b)).

In addition, if the volume fraction of phase 1, f_1, is known, the effective permittivities at points A and B on the above boundaries $\epsilon_{\text{eff}}^{U_0}$

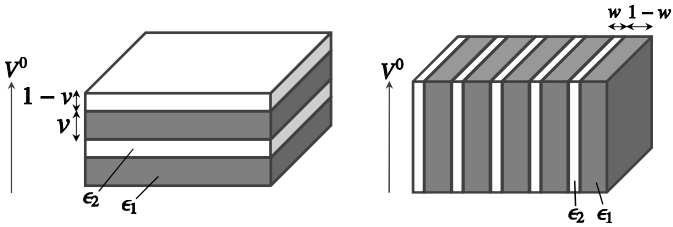

Figure 3. Laminate model.

and $\epsilon_{\rm eff}^{L_0}$ in Figure 2 are determined as follows.

$$\epsilon_{\rm eff}^{A} = \left(\frac{f_1}{\epsilon_1} + \frac{f_2}{\epsilon_2}\right)^{-1} \tag{28}$$

$$\epsilon_{\rm eff}^{B} = f_1\epsilon_1 + f_2\epsilon_2, \tag{29}$$

where $f_2 = 1 - f_1$ is the volume fraction of phase 2. Tighter boundaries are expressed by an arc joining the point A and B that when extended passes through ϵ_2 and an arc that passes through ϵ_1, that can be expressed by the following equations as the parameters v and w are varied from 0 to 1.

$$\epsilon_{\rm eff}^{U_1} = \epsilon_2 + \frac{f_1\epsilon_2\left(\epsilon_1 - \epsilon_2\right)}{\epsilon_2 + vf_2\left(\epsilon_1 - \epsilon_2\right)} \tag{30}$$

$$\epsilon_{\rm eff}^{L_1} = \epsilon_1 + \frac{f_2\epsilon_1\left(\epsilon_2 - \epsilon_1\right)}{\epsilon_1 + wf_1\left(\epsilon_2 - \epsilon_1\right)}. \tag{31}$$

The boundary $\epsilon_{\rm eff}^{U_1}(v)$ represents an elliptic assemblage with a core of component 1 surrounded by component 2 (see Figure 4(a)). On the other hand, the boundary $\epsilon_{\rm eff}^{L_1}(w)$ represents an elliptic assemblage with a core of component 2 surrounded by component 1 (see Figure 4(b)). The major and minor diameters of the phase 1 structure, D_{1a}, D_{1b}, and of the phase 2 structure, D_{2a}, D_{2b}, have following relationship since the inner and outer ellipses are confocal [23].

$$D_{2a}^2 - D_{2b}^2 = D_{1a}^2 - D_{1b}^2. \tag{32}$$

Therefore, volume fraction f_1 and parameter v are described as follows.

$$f_1 = \frac{D_{1a}D_{1b}}{D_{2a}D_{2b}} \tag{33}$$

$$v = \frac{D_{1\rm a}D_{2\rm a}}{D_{1\rm a}D_{2\rm a} + D_{1\rm b}D_{2\rm b}}. \tag{34}$$

Moreover, if we know that the composite is a two-dimensional isotropic material, then we can define the effective permittivities at points X and Y on the above boundaries, $\epsilon_{\rm eff}^{U_1}$ and $\epsilon_{\rm eff}^{L_1}$, respectively, using the following equation.

$$\epsilon_{\rm eff}^{X} = \epsilon_1 + \frac{2f_2\epsilon_1(\epsilon_2 - \epsilon_1)}{2\epsilon_1 + f_1(\epsilon_2 - \epsilon_1)} \tag{35}$$

$$\epsilon_{\rm eff}^{Y} = \epsilon_2 + \frac{2f_1\epsilon_2(\epsilon_1 - \epsilon_2)}{2\epsilon_2 + f_2(\epsilon_1 - \epsilon_2)}. \tag{36}$$

The tighter boundaries are expressed by an arc joining the point X and Y that when extended passes through ϵ_2 and an arc that passes

through ϵ_1. These bounds are expressed by following equations as the parameters v and w are varied from 0 to 1.

$$\epsilon_{\text{eff}}^{U_2} = \epsilon_{\text{eff}}^{X} + \frac{1-v}{1/(\epsilon_{\text{eff}}^{Y} - \epsilon_{\text{eff}}^{X}) + v/(\epsilon_{\text{eff}}^{X} - \epsilon_2)} \tag{37}$$

$$\epsilon_{\text{eff}}^{L_2} = \epsilon_{\text{eff}}^{X} + \frac{1-w}{1/(\epsilon_{\text{eff}}^{Y} - \epsilon_{\text{eff}}^{X}) + w/(\epsilon_{\text{eff}}^{X} - \epsilon_1)}. \tag{38}$$

The boundary $\epsilon_{\text{eff}}^{U_2}(v)$ represents the composite as a cylindrical assemblage with phase 1 as core material and phase 2 as the material surrounding the core (see Figure 5(a)). Similarly, the boundary $\epsilon_{\text{eff}}^{L_2}(w)$ represents the composite as a cylindrical assemblage with phase 2 as core material and phase 1 as the material surrounding the core (see Figure 5(b)).

Apart from the elliptic and cylindrical assemblages [24] there exist a number of other microgeometries that can be shown to realize any material properties on (and within) the bounds. These include so-called rank-n laminates [25–28] and hybrid structures [29]. Excluding multiple microstructural length-scales, so-called Vigdergauz structures have also been shown to attain the bounds in certain cases [30, 31]. Here we also limit ourselves to one length-scale and easily manufacturable microstructures and show that Vigdergauz-like structures are solutions to a variety of different inverse design problems with real and complex effective properties.

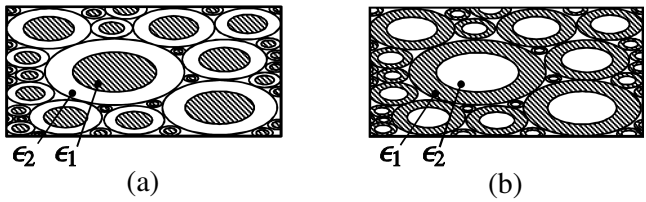

Figure 4. Cross section of the coated elliptic assemblage.

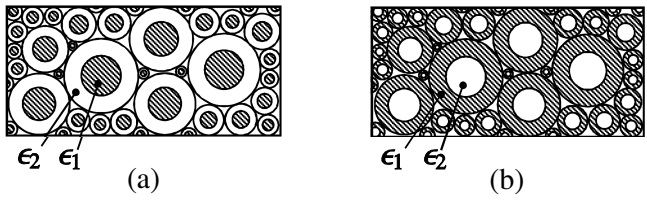

Figure 5. Cross section of the coated cylindrical assemblage.

3.1.2. Bounds of Real Value Effective Permittivity

The bounds of real value effective permittivity versus the volume fraction f_1 is obtained as follows. In the absence of specific information, $\epsilon^A_{\text{eff}}(f_1)$ in Eq. (28) is the lower bound and $\epsilon^B_{\text{eff}}(f_1)$ in Eq. (29) is the upper bound of the effective permittivity of the composite materials versus volume fraction f_1. In addition, if we know the composite is isotropic material, the point $\epsilon^X_{\text{eff}}(f_1)$ in Eq. (35) and $\epsilon^Y_{\text{eff}}(f_1)$ in Eq. (36) are the upper and lower bounds of the effective permittivity of the composite materials versus volume fraction f_1.

3.2. Bounds of 2-D Anisotropic Real Value Effective Permittivity in the Principal Direction When that of the Other Principal Direction Is Known

Based on the discussion in Subsection 3.1, the bounds of the anisotropic effective permittivity in the principal direction when that of the other principal direction is known are derived in this subsection for the case when the dielectric constants of the two materials both have real values. From Eq. (34),

$$1 - v = \frac{D_{1\text{b}} D_{2\text{b}}}{D_{1\text{a}} D_{2\text{a}} + D_{1\text{b}} D_{2\text{b}}} \tag{39}$$

Eq. (34) and Eq. (39) are symmetric with respect to the principal directions, a and b, so $\epsilon(v)$ and $\epsilon(1-v)$ show the effective permittivities of the two principal directions. If we know the permittivity value of one of the principal directions and let it be ϵ^*, the parameter v and w in Eqs. (30) and (31) is obtained as,

$$v^* = \frac{f_1\epsilon_2(\epsilon_1 - \epsilon_2) - \epsilon_2(\epsilon^* - \epsilon_2)}{f_2(\epsilon_1 - \epsilon_2)(\epsilon^* - \epsilon_2)} \tag{40}$$

$$w^* = \frac{f_2\epsilon_1(\epsilon_2 - \epsilon_1) - \epsilon_1(\epsilon^* - \epsilon_1)}{f_1(\epsilon_2 - \epsilon_1)(\epsilon^* - \epsilon_1)}. \tag{41}$$

We then derive the following bounds, substituting $1 - v^*$ and $1 - w^*$ into Eqs. (30) and (31).

$$\epsilon^L_{\text{eff}} = \epsilon_2 + \frac{2f_1\epsilon_2\,(\epsilon_1 - \epsilon_2)}{2\epsilon_2 + (1 - v^*)f_2\,(\epsilon_1 - \epsilon_2)} \tag{42}$$

$$\epsilon^U_{\text{eff}} = \epsilon_1 + \frac{2f_2\epsilon_1\,(\epsilon_2 - \epsilon_1)}{2\epsilon_1 + (1 - w^*)f_1\,(\epsilon_2 - \epsilon_1)}. \tag{43}$$

4. NUMERICAL IMPLEMENTATION

The optimization flowchart is shown in Figure 6. First, the design variables are initialized. Next, the filtered design variable $\tilde{\rho}_e$ is computed using the projection function and the Heaviside function. Objective and constraint functionals are then computed using the FEM. If the objective functional has converged, the optimization procedure is terminated. If not, the sensitivities of the objective and constraint functionals are computed using the AVM. The design variables are then updated using the method of moving asymptotes (MMA) [32] and the process returns to the second step.

5. NUMERICAL EXAMPLES

Numerical examples are now presented to demonstrate the validity and capability of our method for the design of microstructures based on dielectric materials. First, we compare the asymptotic expansion-based and energy-based approaches used to obtain effective permittivity values for the dielectric composites considered here. The following design examples include the design of an isotropic material, an anisotropic material, an anisotropic material with a non-zero off-diagonal terms, and an anisotropic material with loss. The optimization target in all examples is to minimize the square of the difference between the effective permittivity and a target value. The design domain is discretized using 200×200 square elements. A circular rod shape with a volume fraction of 50% is used as the initial configuration unless otherwise specified in the following examples.

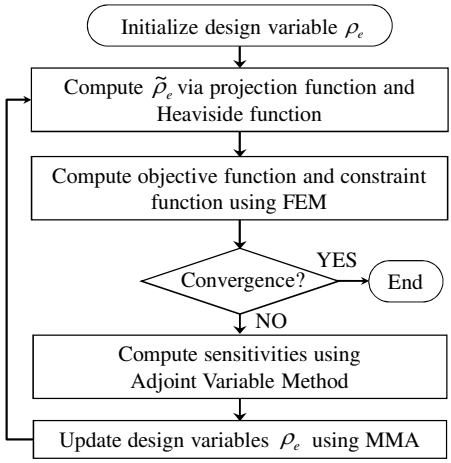

Figure 6. Flowchart of optimization algorithm.

5.1. Comparison of Methods to Obtain Effective Permittivity Values

Here, we compare the asymptotic expansion-based approach and the energy-based approach to show the validity of the energy-based approach used in this paper to obtain effective permittivity values for the dielectric materials. Figure 7 shows a comparison of the effective permittivity values obtained using both approaches for composites made from a single dielectric material with $\epsilon_1 = 100$ and air, ($\epsilon_0 = 1$). Four inclusion shapes with volume fractions of 50% are considered for the comparison. That is, inclusions with a cylindrical hole (Figure 7(a)), cylindrical inclusions (Figure 7(b)), vertically oriented laminates (Figure 7(c)), and vertically oriented laminates rotated 26.57 degrees in the counterclockwise direction (Figure 7(d)) are considered. The effective permeability values obtained using analytic methods are also compared for reference. For a square lattice with cylindrical holes and a lattice with cylindrical inclusions, the Rayleigh formula, defined as follows [33, 34], provides sufficient accuracy.

$$\epsilon_{\text{eff}} = \epsilon_e + \frac{2p\epsilon_e}{\dfrac{\epsilon_i + \epsilon_e}{\epsilon_i - \epsilon_e} - p - \dfrac{\epsilon_i - \epsilon_e}{\epsilon_i + \epsilon_e}(0.3058p^4 + 0.0134p^8)}, \tag{44}$$

where ϵ_i is the permittivity of the cylindrical component, p is its volume fraction, and ϵ_e is the permittivity of the background material. For laminate inclusions, the effective permittivity can be obtained using the Wiener harmonic and arithmetic means (Eqs. (26) and (27)).

$$\epsilon_{\text{eff}} = \begin{bmatrix} 50.5 & 0.0 \\ 0.0 & 1.980 \end{bmatrix}. \tag{45}$$

The effective permittivity values for vertically oriented laminates rotated 26.57 degrees in the counterclockwise direction are obtained by rotating the effective permittivity tensor of the vertically oriented laminates as follows.

$$\epsilon_{\text{eff}} = \begin{bmatrix} \cos\theta & \sin\theta \\ -\sin\theta & \cos\theta \end{bmatrix}^T \begin{bmatrix} 50.5 & 0.0 \\ 0.0 & 1.980 \end{bmatrix} \begin{bmatrix} \cos\theta & \sin\theta \\ -\sin\theta & \cos\theta \end{bmatrix} = \begin{bmatrix} 40.796 & 19.408 \\ 19.408 & 11.684 \end{bmatrix}, \tag{46}$$

where θ is set to 26.57 degrees. We note that analytic methods are valid only for certain inclusion shapes.

For both the asymptotic expansion-based and energy-based approaches, the effective permittivity values are obtained using the FEM. Here, the analysis domain is discretized using 200×200 square elements. The effective permittivity values using the asymptotic expansion-based approach are obtained via following equation.

$$\epsilon^{AS}_{\text{eff},\,ij} = \frac{1}{Y}\int_\Omega \epsilon_r(\mathbf{x})\left(\delta_{ij} + \frac{\partial \chi_j}{\partial x_i}\right) d\Omega, \tag{47}$$

	Analytical method	Asymptotic expansion-based approach $\epsilon_{\text{eff}}^{AS} = \begin{bmatrix} \epsilon_{\text{eff},11}^{AS} & \epsilon_{\text{eff},12}^{AS} \\ \epsilon_{\text{eff},21}^{AS} & \epsilon_{\text{eff},22}^{AS} \end{bmatrix}$	Energy-based approach $\epsilon_{\text{eff}} = \begin{bmatrix} \epsilon_{\text{eff},11} & \epsilon_{\text{eff},12} \\ \epsilon_{\text{eff},21} & \epsilon_{\text{eff},22} \end{bmatrix}$
(a) 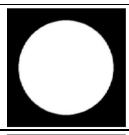	Rayleigh formula $\begin{bmatrix} 33.396 & - \\ - & 33.396 \end{bmatrix}$	$\begin{bmatrix} 32.968 & 0.000 \\ 0.001 & 32.980 \end{bmatrix}$	$\begin{bmatrix} 33.032 & 0.000 \\ 0.000 & 33.032 \end{bmatrix}$
(b) 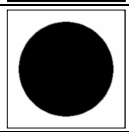	Rayleigh formula $\begin{bmatrix} 2.994 & - \\ - & 2.994 \end{bmatrix}$	$\begin{bmatrix} 3.028 & 0.000 \\ 0.000 & 3.034 \end{bmatrix}$	$\begin{bmatrix} 3.298 & 0.000 \\ 0.000 & 3.298 \end{bmatrix}$
(c) 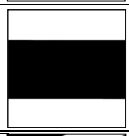	Wiener harmonic and arithmetic means $\begin{bmatrix} 50.5 & 0.0 \\ 0.0 & 1.980 \end{bmatrix}$	$\begin{bmatrix} 50.348 & 0.000 \\ 0.000 & 1.990 \end{bmatrix}$	$\begin{bmatrix} 50.5 & 0.000 \\ 0.000 & 1.980 \end{bmatrix}$
(d) 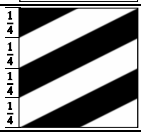	Wiener harmonic and arithmetic means $\begin{bmatrix} 40.796 & 19.408 \\ 19.408 & 11.684 \end{bmatrix}$	$\begin{bmatrix} 40.329 & 19.070 \\ 19.159 & 11.771 \end{bmatrix}$	$\begin{bmatrix} 40.517 & 19.256 \\ 19.256 & 11.623 \end{bmatrix}$

Figure 7. Comparison of effective permittivity values obtained using asymptotic expansion-based and energy-based approaches for composites made from a single dielectric material (black: ϵ_1=100) and air (white: ϵ_0=1). (a) Inclusions with a cylindrical hole. (b) Cylindrical inclusions. (c) Vertically oriented laminates. (d) Vertically oriented laminates rotated 26.57 degrees in the counterclockwise direction.

where Y is the unit cell length and χ_j is obtained by solving following equation with periodic boundary conditions imposed.

$$-\nabla \cdot (\epsilon_r \nabla \chi_j) = \frac{\partial \epsilon_r}{\partial x_j}. \tag{48}$$

As shown in Figure 7, the effective permittivity values obtained using the analytic methods and the asymptotic expansion-based and energy-based approaches are very close for the above four inclusion shapes, demonstrating the validity of the energy-based approach used in this paper.

5.2. Design of Isotropic Material

Here, we consider the design of an isotropic material. The target value is set to $\epsilon_{\text{tar},11} = \epsilon_{\text{tar},22} = 70$. The relative permittivity of the dielectric material is set to 100 and the relative permittivity of the background

material is set to 1. The maximum volume fraction is set to 82.5%, a value chosen from theoretical bounds that will be discussed below.

The optimization results are shown in Figure 8. The obtained effective permittivity is

$$\epsilon_{\text{eff}} = \begin{bmatrix} 70.00 & 0.00 \\ 0.00 & 70.00 \end{bmatrix}. \tag{49}$$

The permittivity values and optimal configuration show that the optimization successfully obtained a clear structure that provides the target permittivity.

Figure 10 shows the theoretical bounds for the effective permittivity of composite materials composed of the above-mentioned dielectric and background materials, where the horizontal axis shows the volume fraction of the dielectric material and the vertical axis shows the effective permittivity of the composite material. The theoretical bounds for anisotropic and isotropic materials are shown by solid and dashed lines, respectively. The effective permittivity of the optimized configuration is shown as the black square in Figure 10 for comparison with the theoretical bound curve, and demonstrates that the obtained result is in good agreement with theoretical bounds.

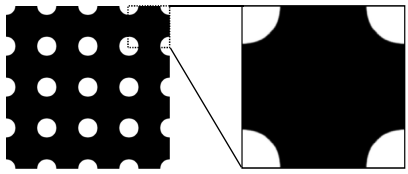

Figure 8. Optimized configuration of the isotropic material design problem for volume fraction $V_{\max} = 0.825$ of $\epsilon_1 = 100$ (black), and $\epsilon_0 = 1$ (white). The targets are $\epsilon_{\text{tar},\,11} = \epsilon_{\text{tar},\,22} = 70$ and the achieved properties are $\epsilon_{\text{eff},\,11} = \epsilon_{\text{eff},\,22} = 70$.

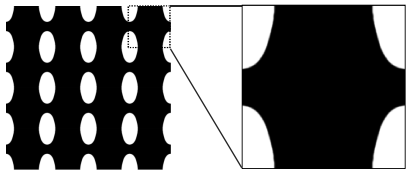

Figure 9. Optimized configuration of the anisotropic material design problem for volume fraction $V_{\max} = 0.76$ of $\epsilon_1 = 100$ (black), and $\epsilon_0 = 1$ (white). The targets are $\epsilon_{\text{tar},\,11} = 45$ and $\epsilon_{\text{tar},\,22} = 70$ and the achieved properties are $\epsilon_{\text{eff},\,11} = 45.00$ and $\epsilon_{\text{eff},\,22} = 70.00$.

5.3. Design of Anisotropic Material

Next, the design of an anisotropic material is considered. The target value is set to $\epsilon_{\text{tar},11} = 45$, and $\epsilon_{\text{tar},22} = 70$. The relative permittivity of the dielectric material is set to 100 and the relative permittivity of the background material is set to 1. The maximum volume fraction is set to 76%, a value chosen from theoretical bounds.

The optimization results are shown in Figure 9. The obtained effective permittivity is

$$\epsilon_{\text{eff}} = \begin{bmatrix} 45.00 & 0.00 \\ 0.00 & 70.00 \end{bmatrix}. \tag{50}$$

The permittivity values and optimal configuration show that the optimization obtained the target permittivity for the anisotropic material to a highly practical extent. Figure 10 shows the theoretical bounds for the effective permittivity. The effective permittivity of the optimized configuration is shown as the black dot in Figure 10 for comparison with the theoretical bound curve. The highly sloped dot-

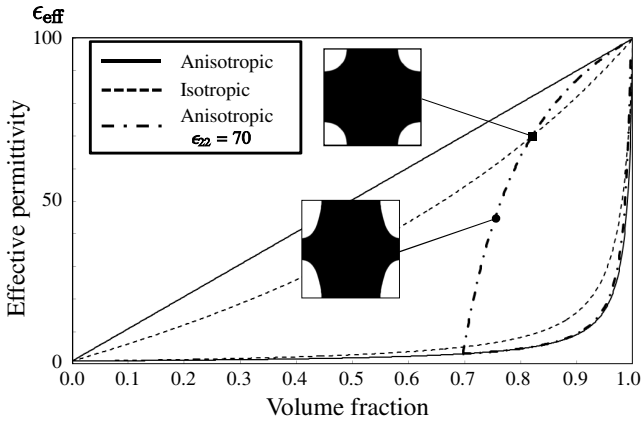

Figure 10. Theoretical bounds for isotropic and anisotropic material design problems with properties $\epsilon_1 = 100$ and $\epsilon_0 = 1$. The solid and dashed lines show the theoretical bounds for isotropic and anisotropic material, respectively. The dot-dashed line plots the upper and lower limit of the permittivity of the anisotropic material versus the volume fraction when $\epsilon_{22} = 70$. The effective permittivity of the optimized configuration, $\epsilon_{\text{eff},11} = \epsilon_{\text{eff},22} = 70.00$, of Subsection 5.2 is shown as the black square, and the effective permittivity of the optimized configuration, $\epsilon_{\text{eff},11} = 45.00$ and $\epsilon_{\text{eff},22} = 70.00$, of Subsection 5.3 is shown as the black dot, for comparison with the theoretical bound curve.

dashed line plots the upper limit of the permittivity of the anisotropic material versus the volume fraction when ϵ_{22} is 70. Similarly, the dot-dashed line that is partially obscured by solid line in the lower right corner of the graph shows the lower limit of the permittivity of the anisotropic material versus the volume fraction when ϵ_{22} is 70. The black dot indicates the effective permittivity value of obtained dielectric materials as optimization results and that the obtained result is in good agreement with theoretical bounds.

5.4. Design of Anisotropic Material with Non-zero Off-diagonal Terms

Here, the design of an anisotropic material with non-zero off-diagonal terms is considered. The target dielectric permittivity is set to

$$\epsilon_{\text{tar}} = \begin{bmatrix} \epsilon_a + \delta\cos 2\phi & \delta\sin 2\phi \\ \delta\sin 2\phi & \epsilon_a - \delta\cos 2\phi \end{bmatrix}, \tag{51}$$

where ϕ is set to 15 degrees and ϵ_a and δ are respectively set to 125 and 40. That is,

$$\epsilon_{\text{tar}} = \begin{bmatrix} 159.64 & -20 \\ -20 & 90.36 \end{bmatrix}. \tag{52}$$

The relative permittivity of the dielectric material is set to 240 and the relative permittivity of the background material is set to 20. The maximum volume fraction is set to 69%, a value chosen from theoretical bounds.

The optimization results are shown in Figure 11. The obtained effective permittivity is

$$\epsilon_{\text{eff}} = \begin{bmatrix} 159.63 & -20 \\ -20 & 90.36 \end{bmatrix}. \tag{53}$$

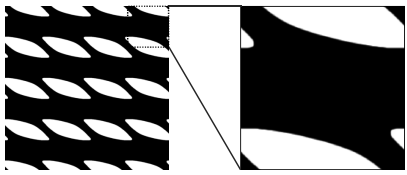

Figure 11. The optimized configuration of the anisotropic material design problem with non-zero off-diagonal terms for volume fraction $V_{\max} = 0.69$ of $\epsilon_1 = 240$ (black), and $\epsilon_0 = 20$ (white). The targets are $\epsilon_{\text{tar},\,11} = 159.64$, $\epsilon_{\text{tar},\,22} = 90.36$ and $\epsilon_{\text{tar},\,12} = \epsilon_{\text{tar},\,21} = -20.00$ and the achieved properties are $\epsilon_{\text{eff},\,11} = 159.63$, $\epsilon_{\text{eff},\,22} = 90.36$ and $\epsilon_{\text{eff},\,12} = \epsilon_{\text{eff},\,21} = -20.00$.

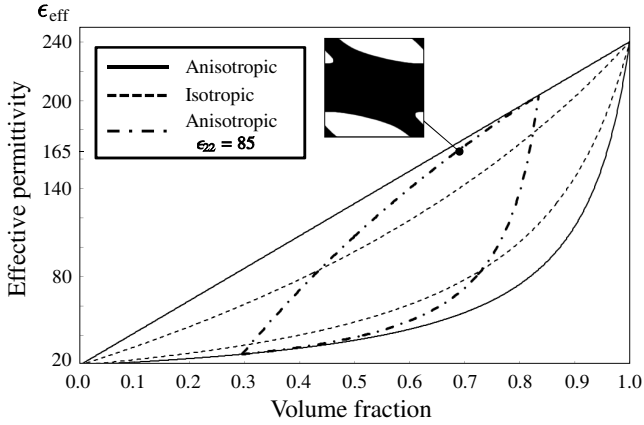

Figure 12. Theoretical bounds for anisotropic material designs with properties $\epsilon_1 = 240$ and $\epsilon_0 = 20$. The solid and dashed lines show the theoretical bounds for isotropic and anisotropic material, respectively. The dot-dashed line plots the upper limit of the permittivity of the anisotropic material versus the volume fraction when $\epsilon_{22} = 85$. The effective permittivity of the optimized configuration, $\epsilon_{\text{eff},\,11} = 164.99$ and $\epsilon_{\text{eff},\,22} = 85.00$, in the principal direction is shown as the black dot for comparison with the theoretical bound curve.

The results show the optimization successfully obtained an optimized configuration that provides the desired permittivity for an anisotropic material that has non-zero off-diagonal terms.

Figure 12 shows the theoretical bounds for the effective permittivity. Here, the obtained effective permittivities in the principal direction are considered, namely,

$$\epsilon_{\text{eff}} = \begin{bmatrix} 164.99 & 0.00 \\ 0.00 & 85.00 \end{bmatrix}. \tag{54}$$

The effective permittivity of the optimized configuration is shown as the black dot for comparison with the theoretical bound curve. The dot-dashed lines plot the upper and lower limit of the permittivity of the anisotropic material versus the volume fraction when ϵ_{22} is 85.

5.5. Design of Material with Loss Targeting Extreme Values

Finally, this design example considers materials with loss. To consider the design of a lossy material, we first consider design problems where target values are known from a theoretical point of view. In these examples, the relative permittivity of the dielectric material is set

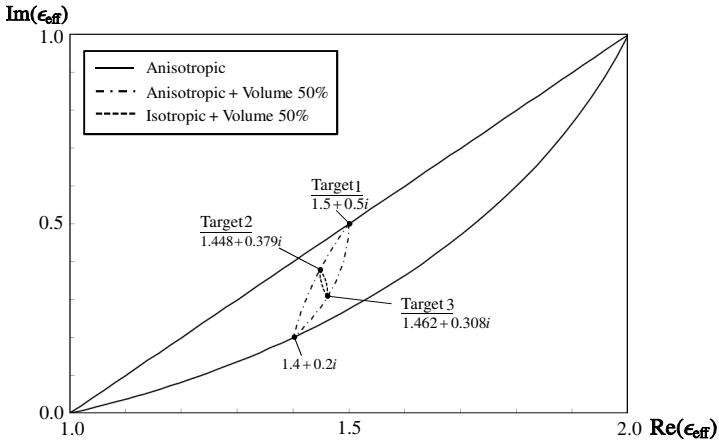

Figure 13. Theoretical bounds for lossy materials with properties $\epsilon_1 = 2 + 1i$ and $\epsilon_0 = 1$. The solid line shows the theoretical bounds for two constituent materials, and the dashed-dot line and dashed line show the theoretical bounds for anisotropic and isotropic material with a volume fraction of 50%, respectively. The black dots indicate the target values used in the optimization in Subsection 5.5.

to $2 + 1i$ and the relative permittivity of the background material is set to 1. The maximum volume fraction is set to 50%. Figure 13 shows the upper and lower bounds for the effective permittivity of composite materials composed of dielectric and background materials. The theoretical bounds for an anisotropic material, an anisotropic material with a volume fraction of 50%, and an isotropic material with a volume fraction of 50% are respectively shown by the solid line, the dot-dashed line, and the dashed line.

Based on these theoretical bounds, three target values were used to validate the present method. As shown in Figure 13, the target values for the three examples were as follows:

For Example 1, the anisotropic material design problem, $\epsilon_{\mathrm{tar},11} = 1.5 + 0.5i$. For Example 2, the isotropic material design problem with maximum loss, $\epsilon_{\mathrm{tar},11} = \epsilon_{\mathrm{tar},22} = 1.4483 + 0.3793i$. And, for Example 3, the isotropic material design problem with minimum loss, $\epsilon_{\mathrm{tar},11} = \epsilon_{\mathrm{tar},22} = 1.4615 + 0.3077i$.

Figures 14, 15 and 16 show the respective optimization results for each example. The obtained effective permittivity in Example 1 is

$$\epsilon_{\mathrm{eff}} = \begin{bmatrix} 1.500 + 0.500i & 0.0 \\ 0.0 & 1.400 + 0.200i \end{bmatrix}. \tag{55}$$

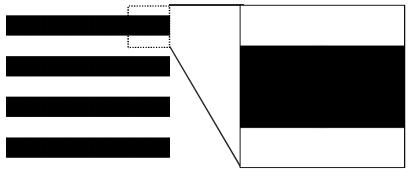

Figure 14. The optimized configuration of a lossy material design problem: target1, for volume fraction $V_{\max} = 0.5$ of $\epsilon_1 = 2 + 1i$ (black — lossy material) and $\epsilon_0 = 1$ (white). The target is $\epsilon_{\text{tar, 11}} = 1.5 + 0.5i$ and the obtained properties are $\epsilon_{\text{eff, 11}} = 1.500 + 0.500i$, $\epsilon_{\text{eff, 22}} = 1.400 + 0.200i$, and $\epsilon_{\text{eff, 12}} = \epsilon_{\text{eff, 21}} = 0.0$.

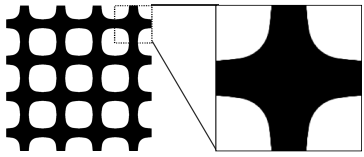

Figure 15. The optimized configuration of a maximum loss material design problem: target2, for volume fraction $V_{\max} = 0.5$ of $\epsilon_1 = 2 + 1i$ (black — lossy material) and $\epsilon_0 = 1$ (white). The target is $\epsilon_{\text{tar, 11}} = \epsilon_{\text{tar, 22}} = 1.448 + 0.379i$ and the obtained properties are $\epsilon_{\text{eff, 11}} = \epsilon_{\text{eff, 22}} = 1.446 + 0.377i$ and $\epsilon_{\text{eff, 12}} = \epsilon_{\text{eff, 21}} = 0.0$.

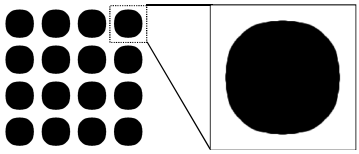

Figure 16. The optimized configuration of a minimum loss material design problem: target3, for volume fraction $V_{\max} = 0.5$ of $\epsilon_1 = 2 + 1i$ (black — lossy material) and $\epsilon_0 = 1$ (white). The target is $\epsilon_{\text{tar, 11}} = \epsilon_{\text{tar, 22}} = 1.462 + 0.308i$ and the obtained properties are $\epsilon_{\text{eff, 11}} = \epsilon_{\text{eff, 22}} = 1.459 + 0.308i$ and $\epsilon_{\text{eff, 12}} = \epsilon_{\text{eff, 21}} = 0.0$.

Although only ϵ_{11} was considered as the target value in the optimization, the obtained value of ϵ_{22} is in good agreement with the theoretical value of ϵ_{22}, that is, $\epsilon_{22} = 1.4 + 0.2i$.

The obtained effective permittivity for Example 2 is

$$\epsilon_{\text{eff}} = \begin{bmatrix} 1.446 + 0.377i & 0.0 \\ 0.0 & 1.446 + 0.377i \end{bmatrix}, \tag{56}$$

and the obtained effective permittivity for Example 3 is

$$\epsilon_{\text{eff}} = \begin{bmatrix} 1.459 + 0.308i & 0.0 \\ 0.0 & 1.459 + 0.308i \end{bmatrix}. \tag{57}$$

These results show that the optimization can successfully find an optimized configuration that has a desired permittivity even for the design of a lossy material.

Observing the optimized structures for maximum damping (Example 2) and minimum damping (Example 3) we note that the results match intuition. For the lossy design, the lossy constituent provides the matrix and the non-lossy is an isolated inclusion — and vise versa.

5.6. Design of Anisotropic Material with Loss: Effect of Initial Configurations

Here, the design of anisotropic materials with loss is considered. The relative permittivity of the dielectric materials is set to $140-0.196i$ and the relative permittivity of the background material is set to $20-0.012i$. Three different initial configurations are used in this design problem. The target values are set to $\epsilon_{\text{tar},11} = 60 - 0.06i$ and $\epsilon_{\text{tar},22} = 70 - 0.08i$.

Figures 17, 18 and 19 show the optimization results based on different initial configurations. Figure 17(a) shows the rod-shaped initial configuration and Figure 17(b) shows its optimized configuration. The volume fraction of the optimized configuration is 60.13%. The obtained effective permittivity is

$$\epsilon_{\text{eff}} = \begin{bmatrix} 59.80 - 0.060i & 0.0 \\ 0.0 & 69.64 - 0.080i \end{bmatrix}. \tag{58}$$

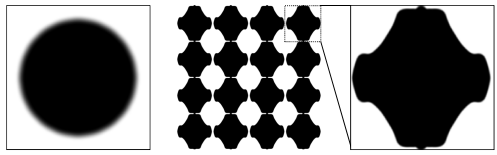

Figure 17. (a) The rod-shaped initial configuration, and (b) the optimized configuration of an anisotropic lossy material design problem, for $\epsilon_1 = 140-0.196i$ (black) and $\epsilon_0 = 20-0.012i$ (white). The target is $\epsilon_{\text{tar},11} = 60.00 - 0.060i$ and $\epsilon_{\text{tar},22} = 70.00 - 0.080i$, and the obtained properties are $\epsilon_{\text{eff, }11} = 59.80 - 0.060i$, $\epsilon_{\text{eff, }22} = 69.64 - 0.080i$ and $\epsilon_{\text{eff, }12} = \epsilon_{\text{eff, }21} = 0.0$.

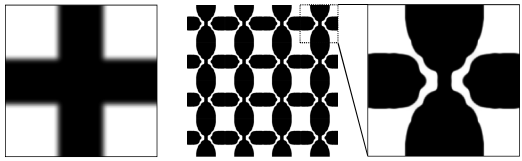

Figure 18. (a) The cross-shaped initial configuration, and (b) the optimized configuration of an anisotropic lossy material design problem for $\epsilon_1 = 140 - 0.196i$ (black) and $\epsilon_0 = 20 - 0.012i$ (white). The target is $\epsilon_{\text{tar},11} = 60.00 - 0.060i$ and $\epsilon_{\text{tar},22} = 70.00 - 0.080i$, and the obtained properties are $\epsilon_{\text{eff, }11} = 59.97 - 0.060i$, $\epsilon_{\text{eff, }22} = 70.00 - 0.080i$ and $\epsilon_{\text{eff, }12} = \epsilon_{\text{eff, }21} = 0.0$.

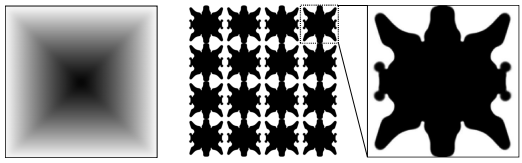

Figure 19. (a) The initial configuration in which the density gradually changes over the design domain, and (b) the optimized configuration of an anisotropic lossy material design problem, for $\epsilon_1 = 140 - 0.196i$ (black) and $\epsilon_0 = 20 - 0.012i$ (white). The target is $\epsilon_{\text{eff, }11} = 60.00 - 0.060i$ and $\epsilon_{\text{eff, }22} = 70.00 - 0.080i$, and the obtained properties are $\epsilon_{\text{eff, }11} = 60.00 - 0.060i$, $\epsilon_{\text{eff, }22} = 69.82 - 0.080i$ and $\epsilon_{\text{eff, }12} = \epsilon_{\text{eff, }21} = 0.0$.

Figure 18(a) shows the cross-shaped initial configuration and Figure 18(b) shows its optimized configuration. The volume fraction of the optimized configuration is 61.50%. The obtained effective permittivity is

$$\epsilon_{\text{eff}} = \begin{bmatrix} 59.97 - 0.060i & 0.0 \\ 0.0 & 70.00 - 0.080i \end{bmatrix}. \tag{59}$$

Figure 19(a) shows the initial configuration in which the density gradually changes over the design domain, from a maximum value at the center ($\rho = 1$) to zero density at the boundaries ($\rho = 0$). Figure 19(b) show the optimized configuration based on this initial configuration. The volume fraction of the optimized configuration is

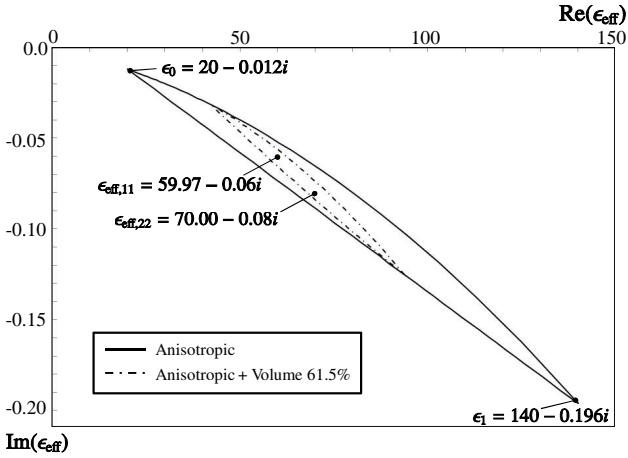

Figure 20. Theoretical bounds of anisotropic lossy material with properties $\epsilon_1 = 140 - 0.196i$ and $\epsilon_0 = 20 - 0.012i$. The solid line shows the theoretical bounds for two constituent materials, and the dashed-dot line shows the theoretical bounds for an anisotropic material with a volume fraction of 61.5%. Two black dots show the effective permittivity of the optimized configuration when using the cross-shaped initial configuration.

61.56%. The obtained effective permittivity is

$$\epsilon_{\text{eff}} = \begin{bmatrix} 60.00 - 0.060i & 0.0 \\ 0.0 & 69.82 - 0.080i \end{bmatrix}. \tag{60}$$

The different optimized structures obtained from the three different initial configurations indicate that this problem has several local optima. Although the obtained optimal values differ slightly from the target value, clear optimized configurations that achieve the prescribed permittivity value are obtained.

Figure 20 shows the upper and lower bounds of the effective permittivity of composite materials composed of the two different lossy dielectric materials. The solid line shows the theoretical bounds for two constituent materials, and the dashed-dot line shows the theoretical bounds for the anisotropic material with loss that has a volume fraction of 61.5%. The two black dots represent the effective permittivity values of the optimized configuration based on the cross-shaped initial configuration. Here, we evaluate only the effective permittivity values obtained in the optimization using the cross-shaped initial configuration, but the evaluations are very similar to those for the other two cases.

6. CONCLUSION

In this paper, we presented a gradient-based topology optimization method that can be applied to the design of microstructures based on a periodic array of dielectric materials to achieve desired electric permittivities. A simple homogenization method was used to obtain the effective permittivity and the validity of the proposed method was demonstrated through several design problems, namely, those dealing with an isotropic material, an anisotropic material, an anisotropic material with a non-zero off-diagonal term, and an anisotropic material with loss. Clear optimized configurations with prescribed electric permittivities were obtained for all the presented cases. Moreover, we derived the theoretical bounds of the two-dimensional anisotropic effective property in the principal direction when the effective property in the other principal direction was set to a prescribed value, to evaluate the effective permittivity values obtained by the optimization. Our results showed that the optimized values are in good agreement with theoretical bounds, confirming that our method yields appropriate and useful solutions.

The Vigdergauz-like optimized structures obtained in this paper provide a directly manufacturable alternative to the multi-length scale microstructures from the literature. The scheme should be directly extendable to three-dimensions, more than two constituents and metamaterial design.

ACKNOWLEDGMENT

This work was partially supported by JSPS, Grant-in-Aid for Scientific Research (B), 22360041, and the "Institutional Program for Young Researcher Overseas Visits." The first author is partially supported by AISIN AW CO., LTD. The third author is partially supported by the Villum Foundation. We sincerely appreciate this assistance.

REFERENCES

1. Bendsøe, M. P. and N. Kikuchi, "Generating optimal topologies in structural design using a homogenization method," *Comput. Methods Appl. Mech. Engrg.*, Vol. 71, No. 2, 197–224, 1988.
2. Yoo, J., N. Kikuchi, and J. L. Volakis, "Structural optimization in magnetic devices by the homogenization design method," *IEEE T. Magn.*, Vol. 36, No. 3, 574–580, 2000.
3. Nomura, T., S. Nishiwaki, K. Sato, and K. Hirayama, "Topology optimization for the design of periodic microstructures composed

of electromagnetic materials," *Finite Elem. Anal. Des.*, Vol. 45, No. 3, 210–226, 2009.

4. Nishiwaki, S., T. Nomura, S. Kinoshita, K. Izui, M. Yoshimura, K. Sato, and K. Hirayama, "Topology optimization for cross-section designs of electromagnetic waveguides targeting guiding characteristics," *Finite Elem. Anal. Des.*, Vol. 45, No. 12, 944–957, 2009.
5. Yamasaki, S., T. Nomura, A. Kawamoto, K. Sato, and S. Nishiwaki, "A level set-based topology optimization method targeting metallic waveguide design problems," *Int. J. Numer. Meth. Eng.*, Vol. 87, No. 9, 844–868, 2011.
6. Borrvall, T. and J. Petersson, "Topology optimization of fluids in stoles flow," *Int. J. Numer. Meth. Eng.*, Vol. 41, No. 1, 77–107, 2003.
7. Sigmund, O. and J. S. Jensen, "Systematic design of phononic band-gap materials and structures by topology optimization," *Phil. Trans. R. Soc. Lond. A*, Vol. 361, 1001–1019, 2003.
8. Sigmund, O. and S. Torquato, "Design of materials with extreme thermal expansion using a three-phase topology optimization method," *J. Mech. Phys. Solids.*, Vol. 45, No. 6, 1037–1067, 1997.
9. Larsen, U. D., O. Sigmund, and S. Bouwstra, "Design and fabrication of compliant micromechanisms and structures with negative Poisson's ratio," *J. Microelectromech. S.*, Vol. 6, No. 2, 99–106, 1997.
10. Sigmund, O., "Materials with prescribed constitutive parameters: an inverse homogenization problem," *INT. J. Solids Struct.*, Vol. 31, No. 17, 2313–2329, 1994.
11. Choi, J. S. and J. Yoo, "Design and application of layered composites with the prescribed magnetic permeability," *Int. J. Numer. Meth. Eng.*, Vol. 82, No. 1, 1–25, 2010.
12. El-Kahlout, Y. and G. Kiziltas, "Inverse synthesis of electromagnetic materials using homogenization based topology optimization," *Progress In Electromagnetics Research*, Vol. 115, 343–380, 2011.
13. Sihvola, A., *Electromagnetic Mixing Formulas and Applicataions*, The Institution of Engineering and Technology, London, 1999.
14. Bensoussan, A., J. L. Lions, and G. Papanicolau, *Asymptotic Analysis for Periodic Structures*, North-Holland Publishing Company, Amsterdam, 1978.
15. Sanchez-Palencia, E., "Non-homogeneous media and vibration theory," *Lecture Notes in Physics*, Vol. 127, Springer-Verlag,

Berlin, 1980.

16. Hashin, Z., "Analysis of composite materials — A survey," *J. Appl. Mech.*, Vol. 50, No. 3, 481–505, 1983.
17. Milton, G. W., *The Theory of Composites*, Cambridge University Press, Cambridge, 2001.
18. Sigmund, O., "On the usefulness of non-gradient approaches in topology optimization," *Struct. Multidisc. Optim.*, Vol. 43, No. 5, 589–596, 2011.
19. Bendsøe, M. P. and O. Sigmund, "Material interpolation schemes in topology optimization," *Arch. Appl. Mech.*, Vol. 69, No. 9–10, 635–654, 1999.
20. Guest, J. K., J. H. Prévost, and T. Belytschko, "Achieving minimum length scale in topology optimization using nodal design variables and projection functions," *Int. J. Numer. Meth. Eng.*, Vol. 61, No. 2, 238–254, 2004.
21. Sigmund, O., "Morphology-based black and white filters for topology optimization," *Struct. Multidisc. Optim.*, Vol. 33, No. 4–5, 401–424, 2007.
22. Olesen, L. H., "A high-level programming-language implementation of topology optimization applied to steady-state Navier-Stokes flow," *Int. J. Numer. Meth. Eng.*, Vol. 65, No. 7, 975–1001, 2006.
23. Milton, G. W., "Bounds on the complex permittivity of a two-component composite material," *J. Appl. Phys.*, Vol. 52, No. 8, 5286–5293, 1981.
24. Hashin, Z., "The elastic moduli of heterogeneous materials," *J. Appl. Mech.*, Vol. 29, No. 1, 143–150, 1962.
25. Francfort, G. and F. Murat, "Homogenization and optimal bounds in linear elasticity," *Archive for Rational Mechanics and Analysis*, Vol. 94, No. 4, 307–334, 1986.
26. Lurie, K. A. and A. V. Cherkaev, "Optimization of properties of multicomponent isotropic composites," *J. Optimiz. Theory App.*, Vol. 46, No. 4, 571–580, 1985.
27. Milton, G. W., *Modelling the Properties of Composites by Laminates*, Vol. 1 of IMA, 150–174, Springer-Verlag, New York, 1985.
28. Norris, A. N., "A differential scheme for the effective moduli of composites," *Mech. Mater.*, Vol. 4, No. 1, 1–16, 1985.
29. Sigmund, O., "A new class of extremal composites," *J. Mech. Phys. Solids*, Vol. 48, No. 2, 397–428, 2000.

30. Grabovsky, Y. and R. V. Kohn, "Microstructures minimizing the energy of a two phase elastic composite in two space dimensions. II: the Vigdergauz microstructure," *J. Mech. Phys. Solids*, Vol. 43, No. 6, 949–972, 1995.
31. Vigdergauz, S., "Energy-minimizing inclusions in a planar elastic structure with macroisotropy," *Struct. Optimization*, Vol. 17, No. 2–3, 104–112, 1999.
32. Svanberg, K., "A class of globally convergent optimization methods based on conservative convex separable approximations," *SIAM J Optimiz.*, Vol. 12, No. 2, 555–573, 2002.
33. Rayleigh, L., "On the influence of obstacles arranged in rectangular order upon the properties of a medium," *Philos. Mag.*, Vol. 34, No. 211, 481–502, 1892.
34. Wallén, H., H. Kettunen, and A. Sihvola, "Composite near-field superlens design using mixing formulas and simulations," *Metamaterials*, Vol. 3, No. 3–4, 129–139, 2009.